ChemComm

COMMUNICATION

View Article Online
View Journal | View Issue

Highly efficient photoelectrochemical water splitting by a hybrid tandem perovskite solar cell†

Abd. Rashid Bin, Mohd Yusoff and Jin Jang*

Cite this: *Chem. Commun.*, 2016, 52, 5824

Received 9th February 2016,
Accepted 15th March 2016

DOI: 10.1039/c6cc01249c

www.rsc.org/chemcomm

Herein, we show that graphene can be fully utilized to function as an electrocatalyst in highly efficient photoelectrochemical water splitting. Combining a solution-processed organic photovoltaic and the state-of-the-art perovskite solar cell in a tandem architecture yields a stable short-circuit water splitting photocurrent of ~7.25 mA cm^{-2} under 1 sun illumination. The ~7.25 mA cm^{-2} photocurrent corresponds to a solar-to-hydrogen efficiency of 9.02%, which is the highest efficiency yet reported for water splitting based on a hybrid tandem perovskite solar cell.

Since we are now facing serious energy shortage and global warming problems, increased awareness on the various environmental problems has led to a shift in the way people go about their life. There has been a change in people's attitudes towards a green lifestyle. People are trying to reduce their impact on the environment. However, this way of life is not widespread and is still evolving. Thus, various alternatives have been put forward to reduce the use of fossil fuels, using wind energy, hydro energy and solar energy. Amongst these clean technologies, solar energy is considered very promising due to its cost, accessibility and inexhaustible amount. In contrast, almost five decades after Fujishima *et al.* proposed the first solar driven electrolysis, utilizing n-type titanium oxide (TiO_2) photoelectrodes in aqueous electrolytes, water splitting received enormous attention from academic and industrial sectors.[1] Inspired by this highly interesting report, researchers have spent decades developing materials and devices capable of converting sunlight into electricity.[2–4] Silcon PVs are the most popular solar cells on the market,[2] and the pilot production of highly efficient photovoltaic modules has already been commercialized. Unfortunately, the high demand for raw materials and high processing and manufacturing costs hinder their large scale production.[5,6] Hence, to overcome this problem there has been a push towards developing a high performance solution-processed organic photovoltaic (OPV).[7,8] To date, multi-junction architectures have been explored to further increase the efficiency of OPV. In multi-junction architectures thermalization and transmission losses are reduced by the absorption of high-energy photons in a wide bandgap absorbing layer and by the absorption of low-energy photons in a narrow bandgap absorbing layer, respectively. Thus, the advancements in multi-junction solar cells have initiated an interesting study by Esiner *et al.* to successfully demonstrate the first PEC water splitting system based on multi-junction OPVs along with a solar-to-hydrogen efficiency of 3.1%.[9] A poor solar-to-hydrogen efficiency is mainly due to a poor power conversion efficiency (PCE) of only 5.3% because they proposed two identical active layers as the middle and bottom cells. Hence, the generated current density (J_{sc}) of the multi-junction OPV was limited by the charge carrier generation of the cells. Nonetheless, this report opened new pathways in developing highly efficient PEC water splitting devices driven by multi-junction OPVs.

Today, the solar-to-hydrogen race is shifted from thin film Si solar cells to perovskite-based solar cells.[10] The perovskite solar cells that use inexpensive solution-processed materials have recently attracted a lot of attention. Surprisingly within less than 6 years, a staggering 21% PCE has been reported.[4] It was reported that perovskite solar cells exhibited promising PCEs along with high open-circuit voltage (V_{oc}) ranging from 0.9 V to 1.5 V,[11–14] which is sufficient for efficient PEC water splitting using vertical piling of two or more solar cells. Accordingly, Luo *et al.* demonstrated a 12.3% solar-to-hydrogen efficiency in their series connected perovskite tandem solar cells employing a bifunctional earth-abundant catalyst with J_{sc} of 10 mA cm^{-2}.[11] In their study, two identical perovskite solar cells were connected in a series leading to a stunning V_{oc} of 2 V and a PCE of 15.7%. Therefore, we considered it be of importance to investigate the possibility of the PEC water splitting device using a tandem configuration by incorporating a wide band-gap semiconducting polymer:fullerene paired with a perovskite planar heterojunction as the bottom and top active layers, respectively. When developing a PEC water splitting device, the standard potential for water splitting is 1.23 V because it provides the thermodynamic driving force. Practically, PEC water splitting takes place at a potential greater than 1.23 V, due to overpotential losses associated with the reaction kinetics. Accordingly, a substantially larger voltage is generally required

Department of Information Display, Kyung Hee University, Seoul, Republic of Korea. E-mail: jjang@khu.ac.kr

† Electronic supplementary information (ESI) available: Device structure, energy diagram, cross-sectional SEM of the tandem device, solar radiation spectrum, *J–V* curves, *J–T* plot, XRD patterns, FTIR spectra, XPS spectra, specific capacitance, and experimental section. See DOI: 10.1039/c6cc01249c

in which it typically operates at a voltage range from 1.4 to 1.9 V.[15] To make things worse, even the best OPVs do not have this potential at their maximum power point and, hence would be unable to provide significant J_{sc} in PEC water splitting.

Here, we demonstrate our findings on the PEC water splitting device using a hybrid tandem perovskite solar cell comprising of an OPV and perovskite solar cell. Our hybrid tandem perovskite solar cell is comprised of a wide band-gap polymer as the bottom cell; poly[(4,4′-bis(3-ethyl-hexyl)dithieno[3,2-b:″3′-*d*]silole)-2,6-diyl-*alt*-2,5-(3-(2-ethyl-hexyl)thiophen-2-yl)thiazolo-[5,4-d]thiazole] (PSEHTT)[16] blended with an indene-C_{60} bis adduct ($IC_{60}BA$)[17] and paired with a perovskite $CH_3NH_3PbI_3$ as the top cell, which is processed using a two-step spin coating method at 100 °C.[10]

Fig. S1a and b (ESI†) show the schematic representation of the complete hybrid device structure and the energy level diagram, respectively. Fig. S2 (ESI†) demonstrates the cross sectional scanning electron microscopy images of our constructed hybrid perovskite tandem solar cells. The current density–voltage (*J–V*) characteristics of the OPV and perovskite solar cells are shown in Fig. 1a under simulated AM 1.5G solar irradiation (100 mW cm^{-2}). The OPV exhibits J_{sc}, V_{oc} and FF of 9.98 mA cm^{-2}, 0.92 V and 0.67, respectively, yielding a PCE of 6.16%. On the other hand, the perovskite solar cell demonstrates J_{sc}, V_{oc} and FF of 19.33 mA cm^{-2}, 1.06 V and 0.72, respectively, resulting in a PCE of 14.89%. The EQE spectra are provided in Fig. 1b. The integrated EQE values are in agreement with the J_{sc} values. The integration of the external quantum efficiency (EQE) spectra with AM 1.5G solar photon flux leads to J_{sc} of 9.42 and 19.01 mA cm^{-2} for the bottom and top solar cells, respectively, in agreement with the values obtained from the *J–V* characteristics. The irradiation spectrum of the light source used in this study is shown in Fig. S3 (ESI†).

The next step was to fabricate a high performance hybrid tandem solar cell that typically requires a robust interconnecting layer (ICL) to recombine holes and electrons from the bottom and top cells, respectively. In the past years, tremendous efforts have been devoted to the development of a chemically robust and highly efficient ICL for the tandem cell.[18] The ICL must be transparent and electrically connect the bottom and top cells allowing the recombination of the holes and electrons from the bottom and top cells, respectively. Furthermore, in order to minimize the potential losses, Ohmic contact between the ICL and the active layers is always desired. Fig. 2a presents the hybrid tandem perovskite solar cell with J_{sc} of 8.73 mA cm^{-2}, V_{oc} of 1.86 V, and FF of 0.72, leading to a record high PCE of 11.28%. The V_{oc} value of the tandem solar cell is in agreement with the summed V_{oc} values of the respective individual values, showing that the bottom and top subcells are efficiently connected. To ensure efficient hydrogen production, the tandem solar cells should provide high J_{sc} and operate near its maximum power point during the PEC water splitting. Thus, the current matching of the subcells is of importance not only in the designing of efficient tandem cells but also to efficiently produce hydrogen. As shown in Fig. S4 (ESI†), the hybrid tandem cells were deposited with bottom subcell thicknesses of 90 and 100 nm, and compared with the tandem cell comprising of the 80 nm thick bottom subcell. V_{oc}'s of the 90 and 100 nm thick bottom subcells remained unchanged by the increased bottom subcell thickness. J_{sc} decreased with increasing bottom subcell thicknesses from 8 mA cm^{-2} to 5.94 and 4.47 mA cm^{-2}, for 90 and 100 nm, respectively. Current matching should enhance J_{sc}, thus one concludes that the hybrid tandem cell better matched the bottom subcell thickness of 80 nm and the bottom subcell became limited by further increasing the bottom subcell thickness. In addition, the operating point J_{sc} of the hybrid tandem perovskite solar cell integrated with PEC water splitting is determined by the meeting point of the *J–V* curves of the hybrid tandem perovskite solar cell and the electrocatalyst (Fig. 2a). The intersection value exhibits a relatively high J_{sc} value of 7.25 mA cm^{-2} and indicates a solar-to-hydrogen efficiency of 9.02%. The relatively high J_{sc} is in agreement with the standalone unbiased light-driven configuration measurement as shown in Fig. 2b, in which it demonstrates the current more clearly within 475 s and 6 hours (Fig. S5, ESI†). The performance of the device is further characterized under AM 1.5G chopped light illumination without applying any external bias for 1 hour (Fig. S6, ESI†). The fluctuation of the current under illumination is caused by bubble formation on the surface, which affects the effective surface area.[14] The overall decrease in current with time is mostly due to the instability of the perovskite solar cell, a challenge that could be addressed by using appropriate encapsulation techniques.

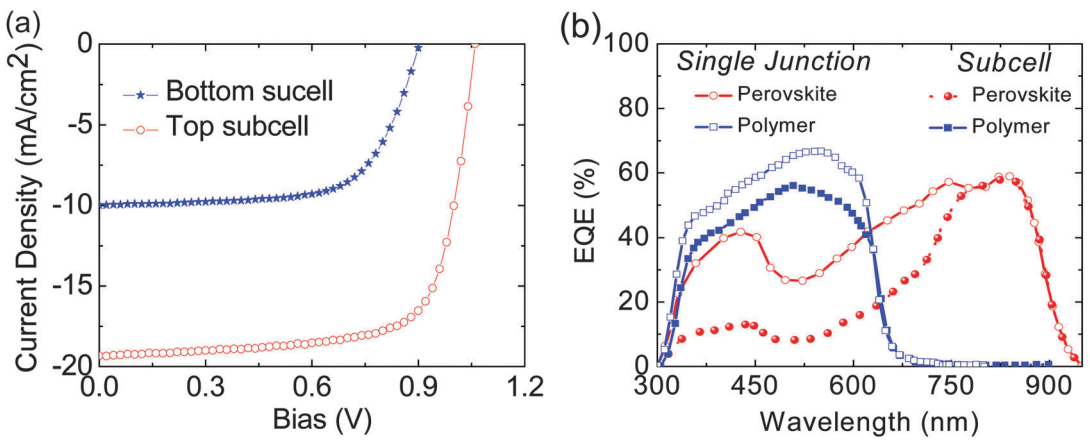

Fig. 1 Device performance. (a) *J–V* characteristics of the OPV (bottom cell) and perovskite solar cell (top cell) under simulated AM 1.5G solar irradiation (100 mW cm^{-2}). (b) The external quantum efficiency of the top and bottom subcells measured in the hybrid tandem device (closed solid lines) and of single junction devices (opened dashed lines).

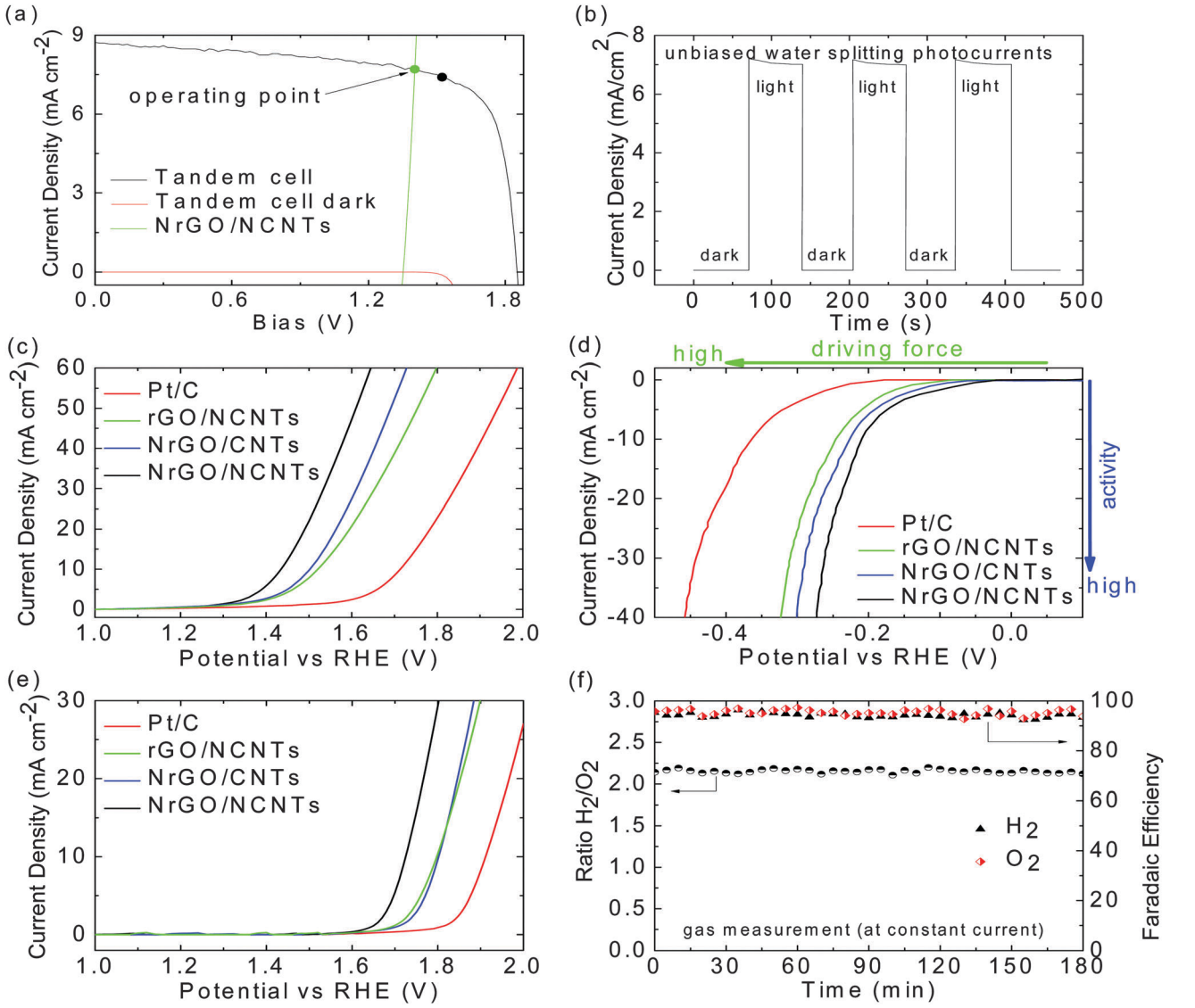

Fig. 2 Efficiency measurement and electrochemical performance with different electrocatalysts. (a) Load-line analysis showing the operating point of a PEC cell as the intersection of the *J*–*V* curve of the hybrid tandem perovskite solar cell and the load curve of the electrochemical components. (b) Current density–time curve of the integrated PEC water splitting without external bias under chopped simulated AM 1.5G 100 mW cm^{-2} illumination. (c) OER characteristics of different electrocatalysts in a three-electrode configuration. (d) Polarization curves comparing their electrocatalytic activity in a three-electrode configuration towards the HER in a 1 mol L^{-1} KOH electrolyte in comparison with that of a Pt/C standard (red trace). (e) Overall PEC water-splitting characteristics of different electrocatalysts in a two-electrode configuration, scanned to 1 V from 2 V. All scan rates were 1 mV s^{-1}. (f) Gas ratio and Faradaic efficiency from gas chromatography measurement of evolved H_2 and O_2 from NrGO/NCNT electrodes in a two-electrode configuration driven by a galvanostat.

Recently, huge progress has been made in identifying electrocatalysts capable of producing oxygen and hydrogen from water. By far, the most efficient electrocatalysts for hydrogen evolution reaction (HER) and oxygen evolution reaction (OER) are still made from metals. Finding stable and efficient electrocatalysts which drive both reactions is difficult, because good catalysts for HER often tend to be poor for OER and vice versa.[19–21] Hence, one of our objectives, besides developing the highly efficient PEC water splitting device, was to develop alternative electrocatalysts that are more abundant and economical. It is worth noting that the electrocatalysts for the HER and OER must be operated in the same acidic or alkaline electrolyte to minimize overpotentials in the electrolyte.[14] The electrocatalytic OER activity of all electrodes was evaluated in a three-electrode system by polarization experiments with potential extended into the water oxidation regime (from 1.00 to 2.00 V). To this end, a film of the as-synthesized nitrogen-doped reduced graphene oxide/nitrogen-doped carbon nanotube (NrGO/NCNT) hybrid was deposited onto a glassy carbon electrode (GCE). In a 1 mol L^{-1} of KOH solution, the NrGO/NCNT catalysts generated a current density of 10 mA cm^{-2} at a much lower potential of 1.43 ± 0.01 V *versus* the reversible hydrogen electrode (RHE) (mean ± s.d, $n = 3$) at a scan rate of 1 mV s^{-1} and with the scan direction to negative from positive.

From the polarization curves, the NrGO/CNT and rGO/NCNT electrocatalysts exhibit a much larger OER onset overpotential of ~1.51 and ~1.53, respectively, to promote the OER current density of 10 mA cm^{-2}. Moreover, the commercially available Pt/C

electrocatalyst required a significantly larger overpotential of 1.72 V in order to reach 10 mA cm^{-2} (0.29 V higher than that of the NrGO/NCNT electrocatalyst) deduced from the corresponding current trend. As noted above, pure CNT and pure rGO did not significantly affect OER activity (Fig. 2c). Therefore, it stands with reason that the exceptional OER activity of the NrGO/NCNT hybrid originated from the nitrogen doping in both layers, where nitrogen served as a synergist. It is also worth noting that a relatively poor performance of Pt/C is due to the low Pt content (20 wt%), which results in a relatively thick cathode layer as well as a low relative humidity on the cathode side (44%) simulating low humidity operating conditions.

Very recent progress in low-dimensional carbon materials, as metal-free catalysts, has shown their promising future in energy-related electrocatalyst OER. In the case of OER, some carbon-based catalysts demonstrated comparable electrocatalytic activity with that of the precious Pt. In general, chemical substitution of some carbon atoms with heteroatoms offers an effective way to tailor its electronic structure and chemical properties. However, current knowledge about electrocatalytic activity for HER on the graphene surface is very inconclusive and the systemic catalysts' molecular design for highly efficient HER is still lacking. Herein, we used the unique structural and functional properties of graphene and CNTs as precursors to synthesize NrGO/NCNT-based electrocatalysts with exceptionally high dual activity in electrocatalyzing both OER and HER. The ability of NrGO/NCNTs to electrocatalyze for HER in alkaline solution was investigated and compared with other electrocatalysts. Fig. 2d presents our attempt to design nitrogen doped rGO and CNT hybrid electrocatalysts with enhanced HER activity to extend the electrochemical application of graphene materials. Fig. 2d reveals the HER polarization curves of various electrocatalysts in 1 mol L^{-1} of KOH solution. rGO/CNT (without any heteroatom doping) has a negligible electrocatalytic activity, while either NrGO or NCNT doping could significantly enhance the HER activity. To achieve a 10 mA cm^{-2} HER current density, the NrGO/NCNT required the overpotential of $\sim$0.015 V, which is lower than that of NrGO/CNT. It is worth noting that the HER activity of the NrGO/NCNTs is comparable to that of some traditional metallic catalysts, such as bulk Au, molybdenum (Mo) and molybdenum/nickel (Mo/Ni) alloys,[22–24] while it is not as good as those of the-state-of-the-art nanostructured molybdenum disulfide/tungsten disulfide (MoS_2/WS_2) and Ni–Mo alloy electrocatalysts. This is perhaps because of the bulky nature and the lack of a large population of active sites because of the stacking rGO and CNT layer during the NrGO/NCNT electrode preparation (drying) process. We attribute the ability of NrGO/NCNTs to catalyze both OER and HER with much higher efficiency than other electrocatalysts due to their unique structure and composition. Fig. 2e demonstrates the overall PEC water splitting in a two-electrode configuration. Generally, the NrGO/NCNT electrocatalyst illustrates superior performance compared with other electrocatalysts, with a 10 mA cm^{-2} PEC water-splitting current reached by applying just 1.72 V. To further verify the bifunctional activity of the NrGO/NCNT electrocatalyst, the evolved gaseous products were evaluated by gas chromatography. Fig. 2f reveals the quantitative Faradaic gas evolution at the predicted 2 : 1 ratio for H_2 and O_2, within experimental error. The exceptional bifunctionality, high activity and low cost of the NrGO/NCNT electrocatalyst make it highly competitive for potential large-scale industrial applications.

In this study, we employed an effective nonprecious electrocatalyst hydrogen evolution reaction and oxygen evolution reaction in an alkaline medium in combination with a tandem hybrid perovskite solar cell for the overall PEC device. This promising combination reports an optimal solar-to-hydrogen conversion efficiency of 9.02%. Through our analysis and the use of the tandem configuration, the device with perovskite and polymer for the top and bottom subcells demonstrates 11.28% power conversion efficiency. With this configuration, we found that light harvesting for the tandem device improved and that given the current state-of-the-art device, tandem configuration (perovskite/polymer) produces the highest photogenerated current density; >7 mA cm^{-2}. In particular, improvements in operating current density using high performance donor materials, new electrocatalysts, and light management are required through device engineering. In addition, the improvement of the photocurrent, especially the onset potential of the photoanode, is needed to fully realize the potential of the tandem OPVPEC device.

This work was supported by MOTIE (Ministry of Trade, Industry & Energy (10052044)) and the KDRC (Korea Display Research Corporation) support program for the development of future device technology for display industry.

References

1 A. Fujishima and K. Honda, *Nature*, 1972, **238**, 37.
2 T. Saga, *NPG Asia Mater.*, 2012, **2**, 96.
3 M. Grätzel, *Nature*, 2001, **414**, 338.
4 http://www.dyesol.com/media/wysiwyg/Documents/2015-asx-announcements/2015-12-08-DYE0397_-_EPFL_achieves_21_efficiency.pdf.
5 N. S. Lewis, *Science*, 2007, **315**, 798.
6 C. A. Wolden, J. Kurtin, J. B. Baxter, I. Repins, S. E. Shaheen, J. T. Torvik, A. A. Rocket, V. M. Fthenakis and W. S. Aydil, *J. Vac. Sci. Technol., A*, 2011, **29**, 030801.
7 A. R. B. M. Yusoff, D. Kim H. P. Kim, F. K. Schneider, W. J. da Silva and J. Jang, *Energy Environ. Sci.*, 2015, **8**, 303.
8 A. R. B. M. Yusoff, S. J. Lee, H. P. Kim, F. K. Schneider, W. J. da Silva and J. Jang, *Adv. Funct. Mater.*, 2014, **24**, 2240.
9 S. Esiner, H. van Eersel, M. M. Wienk and R. A. J. Janssen, *Adv. Mater.*, 2013, **25**, 2932.
10 T. Hamann, *Science*, 2014, **345**, 1566.
11 J. Luo, J. H. Im, M. T. Mayer, M. Schreier, M. K. Nazeeruddin, N.-G. Park, S. D. Tilley, H. J. Fan and M. Grätzel, *Science*, 2014, **345**, 1593.
12 M. G. Walter, E. L. Warren, J. R. McKone, S. W. Boettcher, Q. Mi, E. A. Santori and N. S. Lewis, *Chem. Rev.*, 2010, **110**, 6446.
13 E. Edri, S. Kirmayer, M. Kulbak, G. Hodes and D. Cahen, *J. Phys. Chem. Lett.*, 2014, **5**, 429.
14 E. Edri, S. Kirmayer, D. Cahen and G. Hodes, *J. Phys. Chem. Lett.*, 2013, **4**, 897.
15 S. Ryu, J. H. Noh, N. J. Jeon, Y. C. Kim, W. S. yang, J. Seo and S. I. Seok, *Energy Environ. Sci.*, 2014, **7**, 2614.
16 S. Subramaniyan, H. Xin, F. S. Kim, S. Shoaee, J. R. Durrant and S. A. Jenekhe, *Adv. Energy Mater.*, 2011, **1**, 854.
17 Y. He, H.-Y. Chen, J. Hou and Y. Li, *J. Am. Chem. Soc.*, 2010, **132**, 1377.
18 Y. Yuan, *Green*, 2011, **1**, 65.
19 S. W. Lee, C. Carlton, N. Risch, Y. Surendranath, S. Chen, S. Furutsuki, A. Yamada, D. G. Nocera and Y.-S. Horn, *J. Am. Chem. Soc.*, 2012, **134**, 16959.
20 J. Christensen, P. Albertus, R. S. S. Carrera, T. Lohmann, B. Kozinsky, R. Liedtke, J. Ahmed and A. Kojic, *J. Electrochem. Soc.*, 2012, **159**, R1.
21 V. Nikolova, P. Illiev, K. Petrov, T. Vitanov, E. Zhecheva, R. Stoyanova, I. valov and D. Stoychev, *J. Power Sources*, 2008, **185**, 727.
22 W.-F. Chen, K. Sasaki, C. Ma, A. I. Frenkel, N. Marinkovic, J. T. Muckerman, Y. Zhu and R. R. Adzic, *Angew. Chem., Int. Ed.*, 2012, **51**, 6131.
23 W.-F. Chen, C.-H. Wang, K. Sasaki, N. Marinkovic, W. Xu, J. T. Muckerman, Y. Zhu and R. R. Adzic, *Energy Environ. Sci.*, 2013, **6**, 943.
24 J. Perez, E. R. Gonzalez and H. M. Villullas, *J. Phys. Chem. B*, 1998, **102**, 10931.